Multiphysics Optimization Model to Design High-Power Ultra-High-Speed Machine for Portable Mechanical Antenna Application

Md Khurshedul Islam
Department of Electrical and Computer Engineering
Mississippi State University
Starkville, MS-39762, USA
mi264@msstate.edu

Seungdeog Choi
Department of Electrical and Computer Engineering
Mississippi State University
Starkville, MS-39762, USA
seungdeog@ece.msstate.edu

2021 IEEE Energy Conversion Congress and Exposition (ECCE) | 978-1-7281-5135-9/21/$31.00 ©2021 IEEE | DOI: 10.1109/ECCE47101.2021.9595765

***Abstract*—This paper presents a new Multiphysics optimization strategy to design a high-power ultra-high-speed machine (HP-UHSM). The design process of HP-UHSM is highly iterative and requires Multiphysics optimization to deal with different critical design challenges such as windage loss, thermal limit, centrifugal force, and vibration. However, the Multiphysics optimization of HP-UHSM is a challenge due to several design variables and the huge computation cost of finite element analysis (FEA). In this paper, an integrated Multiphysics optimization process is developed using a combined FEA and analytical model, which provides a robust design geometry and significantly reduces the computational cost. The optimization process integrates a parameterized FEA electromagnetic module with analytical models of thermal, structural, and Rotordynamic analysis. Therefore, it can apply multi-disciplinary design constraints from application requirements and the material's limitations. The optimal result ensures an efficient and feasible design with a high design-safety-margin by considering the Multiphysics mutual influence. To investigate the efficiency of the proposed optimization model, a 2 kW 500 krpm permanent magnet synchronous machine is designed considering some unique requirements of a potable mechanical antenna. The multi-disciplinary performance of the designed machine is studied using 3-D FEA and experimental analysis to evaluate the accuracy and computational efficiency of the proposed model. The comparative results confirm that the proposed optimization model can design an efficient and robust HP-UHSM with high accuracy and very low computational cost.**

Keywords—Analytical model, critical speed, Multiphysics optimization, permanent magnet machine, stress, ultra high speed.

I. Introduction

In recent years, the demand for high-power ultra-high-speed machine (HP-UHSM) machines is increasing in many new emerging applications such as the portable mechanical antenna, machine tool industry, portable charger, and medical application [1]-[3]. The most attractive features of UHSM are high power density, compact structure, and high efficiency. However, increasing the torque rating of UHSM makes its design process more complicated, especially in structural integrity, temperature limit, critical frequency, and prototyping. Moreover, the mutual influence between the electromagnetic, thermal, mechanical, and Rotordynamic performances become stronger, especially at ultra-high-speed (UHS). Therefore, Multiphysics optimization is highly recommended to design an HP-UHSM by addressing these issues.

Finite-element analysis (FEA) is a powerful, accurate, and preferred platform for designing electric machines and their performance analysis [4]. However, it is very time-consuming due to the need for high-precision mesh generation [5]. Consequently, a complete FEA-based Multiphysics optimization will require enormous computational power and time because it is a highly iterative process and has a higher number of design variables. This problem becomes even worse if different physics models are coupled to each other for considering Multiphysics performance influence at every design point. Therefore, the FEA-based Multiphysics optimization of HP-UHSM is a challenge considering the design time and computational cost. The efficient solution to this problem is to use an analytical model for Multiphysics optimization of HP-UHSM. Since UHSMs use a simple machine geometry compare to the conventional electrical machine, an accurately developed analytical model can provide a good result.

In literature, analytical model-based optimization has been used for UHSM design. The machine has an operating speed of ~500 krpm or more is our interest. In [6], a 100 W 500 krpm machine is designed using an analytical model of total loss minimizing optimization. A similar approach is used in [7] to design a 300 W 500 krpm slot-less self-bearing permanent magnet motor. In [8], another 100 W 500 krpm UHSM is designed by a combined optimization approach, which utilizes both the FEA and analytical model. It uses the specific mass and electrical loss minimizing approach while the cost function includes the different electromagnetic constraints and the rotor stress constraints. The author also claims that the optimization model can design low-torque UHSM up to 1.2 million rpm.

However, all of these models are developed to design low-torque (1 to 6 mNm) UHSM, and the optimization model includes mostly electromagnetic constraints. Apart from this, the model of [6] and [7] do not consider the mutual influence of electromagnetic, thermal, and structural performance. They also assume that the stator winding has no influence on the magnetic field generation, no magnetic saturation in the stator core, and ignores the non-linear electromagnetic characteristics of active-part material. Though the model of [8] uses FEA for electromagnetic analysis, it designs the rotor and the stator individually where the rotor is sized mainly based on the windage loss, and stator is designed for specific electromagnetic efficiency. It does not consider the electromagnetic influence of rotor and stator design parameters simultaneously. It also ignores the mutual impact of electromagnetic loss on the temperature rise for different design parameters. Moreover, none of these models consider the rotor's critical frequency and its vibration limit in the optimization. Consequently, these analytical optimization models are not suitable for designing an HP-UHSM because increasing the torque requirement at the UHS introduces several additional multi-disciplinary design constraints other than the electromagnetic constraints. It includes the rotor stress limit, maximum magnet temperature limit, uneven magnet axial temperature variation, critical bending frequency below the rated frequency, and several

manufacturing constraints. Also, the mutual influence of different physics performances becomes highly correlated.

In this paper, a new Multiphysics optimization strategy is presented to design an HP-UHSM. It includes the electromagnetic, thermal, structural, and Rotodynamic analysis model to consider the multi-disciplinary design constraints of HP-UHSM. The different physics models are coupled to reflect the Multiphysics performance influence for each design point. Also, using the proposed model, a 2 kW 500 krpm UHS permanent magnet synchronous motor is designed for portable mechanical antenna application.

II. Developing Analytical Models for HP-UHSM

UHSM requires a simple and robust design geometry to survive mechanically at UHS rotation. Therefore, when the rated speed goes more than 200 krpm, they share almost similar design geometry, for example, 2-pole shrink-fitted rotor and slot-less stator to reduce the high-frequency operating loss. Fig. 2 shows the 2-D cross-section of the studied HP-UHMS.

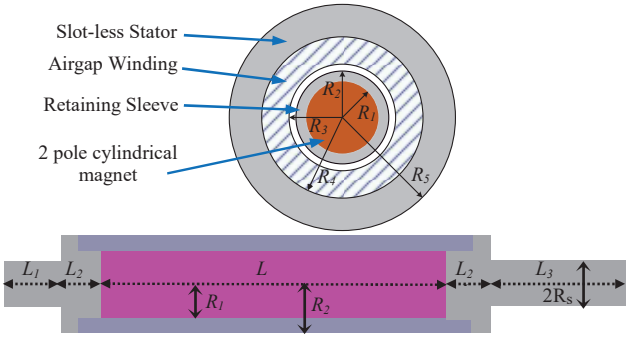

Fig. 1: (Top) 2-D cross-section, (bottom) axial cross-section of the studied HP-UHSM geometry. [not drawn in scale]

A. Electromagntic Model

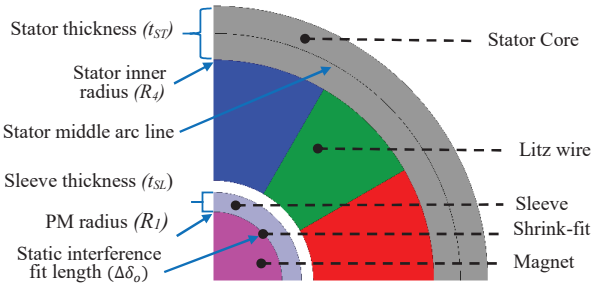

Fig. 2: 2-D parametric finite element electromagnetic model (1/4th).

In HP-UHSM, accurate estimation of electromagnetic performance is crucial, especially the electromagnetic losses for thermal analysis and flux density to avoid material saturation. Hence, an electromagnetic FEA is used to calculate the electromagnetic losses, core flux density, current density, average torque, and material saturation. It can also consider the non-linear electromagnetic characteristics of the active part material. The electromagnetic model is developed on the ANSYS Electronics Desktop platform. Fig. 2 shows the 2-D parametric electromagnetic model, where the ANSYS design-symmetry feature is applied to reduce the computational time. Nine machine sizing variables are selected, including the input current, number of phases, number of turns per phase, and geometry parameters shown in Fig. 2. Output variables of this model are the electromagnetic torque, stator core flux density, copper loss, rotor loss, core loss, and current density. The average torque of one revolution is defined as the output torque. The peak flux density on arc line at the last simulation time is defined as core flux density. The current density is calculated as (1):

$$J_{den} = \frac{I_a N_c}{K_f A_s} \tag{1}$$

where I_a is the input phase current (RMS), N_c is the number of turns per phase, K_f is the slot fill factor, and A_s is the cross-section area of a coil side.

In an HP-UHSM, the copper loss can be divided into the conduction loss ($P_{cu\text{-}s}$) and the proximity loss ($P_{cu\text{-}p}$) as (2):

$$P_{cu} \approx P_{cu-skin} + P_{cu-prox} \tag{2}$$

The total conduction loss of winding caused by the skin effect is calculated as (3):

$$P_{cu-skin} = m I_a^2 R_{dc,p} \tag{3}$$

where m is the number of phases and $R_{dc,p}$ is the per phase DC resistance of Litz wire, which is calculated as (4):

$$R_{dc,p} = \frac{4\rho_{cu} l_{cu}}{n d^2 \pi} \{1 + \alpha_{cu}(T_W - T_o)\} \tag{4}$$

where n is the number of parallel strands or conductors, d is the strand diameter, l_{cu} is the total conductor length, ρ_{cu} is the copper resistivity, α_{cu} is the copper conductivity, T_w is the winding temperature, and T_o is the room temperature.

According to [9], the proximity loss of the slot-less HP-UHSM is calculated using (5):

$$P_{cu-prox} = \frac{B_{p,cu}^2 \omega^2 d^2 \sigma_{cu}}{32} V_{cu} \tag{5}$$

where ω is the electrical angular frequency, $B_{p,cu}$ is the peak flux density, and V_{cu} is the total volume of the airgap winding.

The simplified Bertotti iron loss reparation model [10] is used to accurately calculate the core loss in the stator as (6):

$$P_{iron} = P_{hy} + P_{ed} + P_{ex} = k_h f B_{p,s}^2 + k_c f^2 B_{p,s}^2 + k_e \left(f B_{p,s}\right)^{3/2} \tag{6}$$

where, P_{hy} is the hysteresis loss, P_{ed} is the eddy current loss, and P_{ex} is the excess loss, $B_{p,s}$ is the peak flux-density of the stator core; $k_h, k_c, and\ k_e$ are the different loss coefficient of the core material. In ANSYS, "Core loss vs frequencies" technique is used to calculate these loss coefficients.

In HP-UHSM, the rotor power loss is mainly due to the eddy current loss generates in the sleeve and PM. This loss is calculated using ANSYS post-processing capability as (7):

$$P_{rotor} = \int_V \sigma E^2 dV \tag{7}$$

where σ is the material conductivity, E is the electric field applied of the rotor, and V is the effective rotor volume.

B. Windage Loss Model

In HP-UHSM, windage loss is the most dominant part of the machine's overall losses at UHS rotation. This loss reduces the efficiency and affects the rotor temperature distribution significantly. The windage loss of a cylindrical rotor enclosed by a hollow stator can be calculated accurately using (8):

$$P_{windage} = \pi C_r C_d \rho_{air} \omega^3 R_2^4 l_r \quad (8)$$

where ρ_{air} is the air density, ω is the mechanical rotation speed, R_2 is the outer rotor radius, and l_r is the rotor axial length exposed to the air-gap. C_r is the roughness coefficient of the rotor surface. For a smooth rotor surface, $C_r = 1$. C_d is the drag coefficient, depends on the rotor geometry and airflow behavior. The airflow behavior of the studied rotor can be determined using the Taylor number, defining as (9):

$$Ta = \frac{r_0 \omega \rho_{air} R_2}{\mu} \sqrt{\frac{r_o}{R_2}} \quad (9)$$

Where r_o is the airgap length, and μ is the dynamic viscosity of air. According to [11], the airflow is classified as laminar-Couette, Laminar flow with Taylor vortices, and turbulent flow if $Ta < 41.3$, $41.3 < Ta < 440$, and $Ta > 440$, respectively. For laminar-Couette flow, C_d is calculated as (10):

$$C_d = \frac{1.8}{R_e} \left(\frac{r_o}{R_2}\right)^{-0.25} \frac{(R_2+r_o)^2}{(R_2+r_o)^2 - R_2^2} \quad (10)$$

where R_e is the Reynolds number, calculated as (11):

$$Re = \frac{\rho \omega R_2^2}{\mu} \quad (11)$$

For a UHSM, especially when the rated speed is around 500 krpm, the airflow is always turbulent. At this point, the windage loss increases dramatically, and accurate calculation of C_d is difficult. According to empirical equation [12], the C_d can be estimated using (12):

$$C_d \propto Ta^{-0.2} \quad (12)$$

However, for HP-UHSM, accurate estimation of C_d is highly recommended because it is directly proportional to the windage loss. The computational fluid dynamic (CFD) analysis can be used to calculate the C_d more accurately. For CFD analysis, C_d can be defined as (13):

$$C_d = \frac{Shear\ stress\ on\ the\ rotor\ surface}{Dynamic\ Pressure} \quad (13)$$

C. Thermal Model

HP-UHSM experiences a high operating temperature at UHS due to its high loss-per-unit area. However, the operating temperature in the permanent magnet (PM) and winding are strictly limited by the maximum energy product (BH_{max}) and insulation type, respectively. The PM temperature rise also influences the structural deformation and windage loss of the rotor. Therefore, during the optimization, these temperatures must be calculated and observed their impact on the other performances. To do that, a lumped parameter thermal model (LPTM) of the full machine is developed and integrated into the optimization model. Fig. 3 shows the simplified LPTM of the studied HP-UHSM, where current sources represent the heat sources generated by the corresponding loss and voltage source represent the ambient temperature. The equivalent thermal resistances depend on the machine geometry and corresponding material property [13]. Ten nodes represent the temperature of different parts. For simplification, the heat transfer by means of conduction and convection are considered here, while the negligible heat transfer by radiation is ignored. The losses are imported from

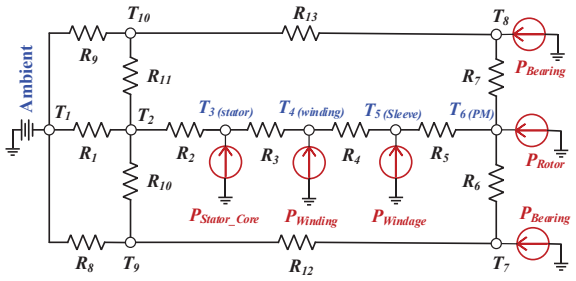

Fig. 3: Simplified lumped parameter thermal model (LPTM) of HP-UHSM.

the electromagnetic and windage loss model. The bearing loss mainly depends on the bearing type, reloading, application, and rotational speed of the rotor. In this case, two ball bearings are considered, and their power loss is estimated using the empirical model as (14), validated in [14]:

$$P_{bearing} = c_4 \left(\frac{Rotating\ frequency}{1\ Hz}\right)^{c_5} \quad (14)$$

where c_4 and c_5 are two empirical constants.

The heat transfer coefficients (HTC) are calculated using the machine geometry, materials properties, and rotational speed. The HTC on the airgap rotor surface is calculated as (15):

$$h_{air-gap} = Nu * \frac{\rho_{air}}{2 \times r_o} \quad (15)$$

where Nu is the Nusselt number, defined as [15]:

$$Nu = \begin{cases} 2 & ; 0 < Ta < 1740 \\ 0.409\, T_a^{0.241} - 137 Ta^{-0.75}; & Ta \geq 1740 \end{cases} \quad (16)$$

with Ta is the Taylor number (17):

$$Ta = \frac{\omega^2 r_{ag} r_o^3}{v_{air}^2 C_r} \quad (17)$$

where ω is the rotor angular velocity, r_{ag} is the average airgap length ($r_{ag} = (R_2+R_3)/2$), and v_{air} is the air kinematic viscosity.

The HTC on the non-airgap rotor surface is calculated from the Nusselt number and Taylor Number as (18) [16]:

$$\left.\begin{aligned} h_{non-air-gap} &= \frac{Nu_o \times \rho_{air}}{R} \\ Nu_u = 0.0628 \times Re^{0.7}, \ \text{and} \ \ Re &= \frac{2\pi\omega R^2}{60\, v_{air}} \end{aligned}\right\} \quad (18)$$

D. Structural Model

The mechanical stress of the UHS rotor due to its excessive centrifugal force is one of the major limiting factors of HP-UHSM design. The rear-earth PM is a fragile material and has a low flexural strength. Though a high-strength retaining sleeve is used to protect the PM, there should always be a suitable safety margin of the developed stress to ensure a reliable operation at UHS. Therefore, accurate calculation of rotor stress during optimization is very important. To do that, an analytical model is developed for the studied HP-UHSM based on the stress equilibrium theory of rotating disk [17]. In the studied rotor structure shown in Fig. 1 has three primary sources of mechanical stress and displacement:

i. Contact pressure due to the shrink-fit

The shrink-fit technique is used to implement an interference fit between the PM and sleeve to secure a rigid

and safe assembly between them. It is also essential to ensure a proper transfer of the developed torque from the PM to the rotor shaft. A possible technique of shrink-fitting is heated up the sleeve and cooled down the PM. Then, install the PM into the sleeve, which has a smaller inner radius compare to the outer radius of the PM. The applied radial static shrink-fit can be calculated as:

$$\Delta\delta_o = R_{pm,o} - R_{sl,i} \tag{19}$$

where $R_{pm,o}$ is the outer magnet radius and $R_{sl,i}$ is the sleeve inner radius. In this technique, the maximum possible $\Delta\delta_o$ depends on the allowable material temperature (T_{Sleeve}, T_{PM}), coefficient of thermal expansion (CTE) (α_{th}), and the PM radius (R_1) as shown in (20):

$$\Delta\delta_{o,max} = \alpha_{th} R_1 (T_{Sleeve} - T_{PM}) \tag{20}$$

Also, the mechanical stress and displacement of both the PM and sleeve are influenced by the static shrink-fit length. It should be selected such that the developed von misses stress on both PM and sleeve remains below their corresponding yield strength limit considering a desired design safety margin (DSM). At the rotating condition, the dynamic shrink-fit length can be determined by (21), and the developed contact pressure at the shrink fit zone is calculated by using (22)

$$\Delta\delta = u_m + u_s - \Delta\delta_o \tag{21}$$

$$p_c = \frac{\Delta\delta E_m E_s (R_2^2 - R_1^2)}{E_S\left[(R_1^3 - R_1 R_2^2)v_m - R_1^3 + R_1 R_2^2\right] + E_m\left[(R_1 R_2^2 - R_1^3) + R_1^3 + R_1 R_2^2\right]} \tag{22}$$

To ensure torque transfer at UHS, p_c must be positive.

ii. Centrifugal stress due to the rotating speed

During the rotating condition, the radial (σ_r) and tangential (σ_t) stress developed in the UHS rotor is derived using the static equilibrium equation, which converts the dynamic disc problem into a steady-state equilibrium as (23):

$$u = \frac{1}{E}\left(k_1 r(1-v) - k_2 \frac{1}{r}(1+v) - \frac{1-v^2}{8}\rho r^3 \omega^2\right) \tag{23}$$

where u is the radial displacement, r is the distance from the center, ρ is the material density, ω is the angular velocity, k_1, and k_2 are the constants. By using inverted Hooke's law and strain-displacement relation, σ_r and σ_t is derived as (24):

$$\left.\begin{aligned} \sigma_r &= k_1 + k_2 \frac{1}{r} - \frac{3+v}{8}\rho r^2 \omega^2 \\ \sigma_t &= k_1 - k_2 \frac{1}{r^2} - \frac{1+3v}{8}\rho r^2 \omega^2 \end{aligned}\right\} \tag{24}$$

iii. Thermal expansion due to the rotor temperature

When the rotor is running at UHS, the rotor temperature rises considerably due to the excessive windage loss. Since both the PM and sleeve material have a positive CTE, their mechanical displacement will be affected by the rising temperature, which will further affect the stress development. The material expansion (u_i) due to the temperature rise is calculated by using (25) and integrated into (23):

$$u_i = \alpha_{th_i} r\,(T_{m\_i} - T_o) \tag{25}$$

where T_{m_i} is the maximum temperature of i = PM or sleeve.

The total radial displacement and mechanical stress on PM and sleeve due to the shrink-fit pressure, rotational speed, and temperature is calculated simultaneously as a function of r as:

$$\left.\begin{aligned} u_i(r) &= \frac{1}{E_i}\left(k_{1,i} r(1-v_i) - k_{2,i}\frac{1}{r}(1+v_i) - \frac{1-v_i^2}{8}\rho_i r^3 \omega^2\right) \\ &\quad + \alpha_{th,i} r\left(T_{max,i} - T_o\right) \\ \sigma_{r,i}(r) &= k_{1,i} + k_{2,i}\frac{1}{r} - \frac{3+v_i}{8}\rho_i r^2 \omega^2 \\ \sigma_{t_i}(r) &= k_{1,i} - k_{2,i}\frac{1}{r^2} - \frac{1+3v_i}{8}\rho_i r^2 \omega^2 \end{aligned}\right\} \tag{26}$$

The constants $k_{1,PM}$, $k_{2,PM}$, $k_{1,SL}$, and $k_{2,SL}$ are calculated using the following boundary conditions (27):

$$\left.\begin{aligned} u_{PM}(r=0) &= 0 \\ \sigma_{r,SL}(r=R_2) &= 0 \\ \sigma_{r,PM}(r=R_1) &= \sigma_{r,SL}(r=R_1) \\ u_{SL}(r=R_1) - u_{PM}(r=R_1) &= \Delta\delta_o \end{aligned}\right\} \tag{27}$$

The von Misses equivalent stress (VMES) criterion is used to calculate yield stress, and the VMES is defined as (28):

$$VMES_i = \sqrt{(\sigma_{r,i} - \sigma_{t,i})^2 + \sigma_{r,i}.\sigma_{t,i}} \tag{28}$$

E. Rotordynamic Model

In HP-UHSM, any critical bending frequency below the fundamental operating frequency must be avoided to secure the UHS rotor from excessive vibration and mechanical breakdown. In the proposed optimization process, the first-order bending frequency of the studied rotor is estimated using an analytical model and restricted it above the fundamental frequency. The undamped natural frequency of a cylinder beam shaft can be calculated using (29):

$$\omega_n = \alpha_n \sqrt{\frac{Er^2}{64\rho L^4}} \tag{29}$$

where E is Young's modulus and ρ is the mass density of the material, r is the radius and L is the length of the shaft, and α_n is a series constant of n_{th} natural frequency, depending on the rotor's physical properties and boundary conditions. Equation (29) can be modified for the studied rotor geometry as (30):

$$\omega_n = \sqrt{\frac{(1/256)a_n^2 E R_2^4}{\left[\rho_{SL}\left\{R_S^2 L_1^4 + R_S^2 L_3^4 + 2R_2^2 L_2^4 + (R_2 - R_1)^2 L^4\right\} + \rho_{PM} R_1^2 L^4\right]}} \tag{30}$$

where ω_n is the nth natural frequency, R_1, R_2, R_s, L, L_1, L_2, and L_3 are rotor dimensions as shown in Fig. 2, ρ_{SL} and ρ_{PM} are the mass density of the sleeve and PM material, respectively.

III. Multiphysics Optimization Model

The combined Multiphysics optimization model is developed in the ANSYS Workbench platform. The abovementioned analytical models are written using the excel script feature of Workbench. Fig. 4 shows the simplified framework of the proposed optimization model. It starts with initial consideration and can optimize the active part materials as well as multi-phase winding configuration. It couples a 2-D Electronics desktop module with analytical models using the parameter set feature to consider the influence of Multiphysics performance variation. A response

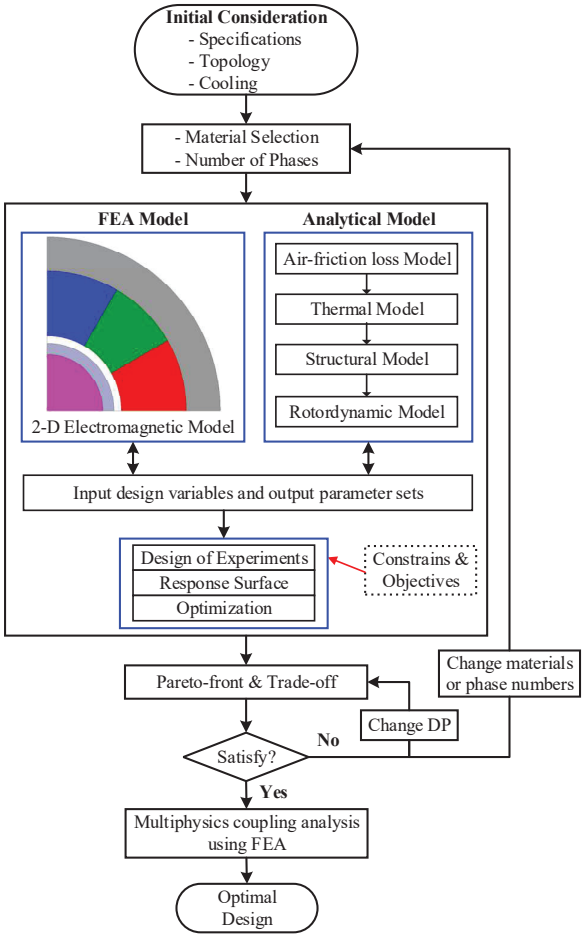

Fig. 4: Proposed Multiphysics optimization strategy.

surface optimization (RSO) module is connected with the parameter set module to perform the optimization. In RSO, first, the design of experiment (DOE) technique is used to generate initial samples for each input design parameter. Then, the response surfaces are created using these samples by applying the Kriging method. From the response surface result, the global parameter sensitivity can be analyzed to evaluate the influence of each input design parameter on different output parameters and design objectives. It helps to decrease the number of design variables based on their impact on the output parameters. Then, the constraints and objective functions are defined in the optimization according to application requirements and practical considerations.

When the optimization model requests a new design point (DP), first the FEA electromagnetic simulation is solved, and then the analytical models are evaluated sequentially, as shown in Fig. 4. The thermal model uses the windage loss, bearing loss, and electromagnetic losses as the input heat source for the corresponding DP. The calculated PM and sleeve temperature are then used in the structural model to obtain the material's thermal expansion. Once all the DPs are solved, the Pareto-front can be obtained based on the defined constraints and optimization result. Then, the optimal design which satisfies all the multi-physics constraints and has the highest DSM is searched from the Pareto-front solutions by an appropriate trade-off. If no DP is found with a desire DSM,

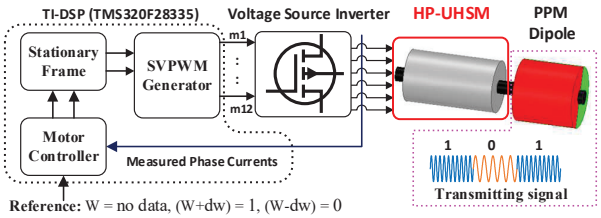

Fig. 5: Simplified illustration of AMEBA system using an HP-UHSM.

change the materials or number of phases. If a desire DP is found, a Multiphysics coupling analysis using the FEA model is performed to finalize the geometry parameters for prototyping.

IV. Design of 2 kW 500 krpm UHSM

Using the proposed optimization model, an HP-UHSM is designed in this section. The motor will be used in a mechanical-based antenna (AMEBA) system. AMEBA is a new concept of wireless communication in the RF-denied environment using extremely-very low frequency (ELF-VLF) generated by a mechanical transmitter. This electro-mechanical transmitter concept received significant academic attention since it was first described in 2017 by the DARPA AMEBA program [18]. Our previous works [19-20] present the possibility and effectiveness of using a rotating permanently polarized magnet (PPM) dipole in the AMEBA system, shown in Fig. 5. It uses a high-speed motor drive for rotating a PPM dipole to generate an alternating magnetic field at ELF-VLF. As a result, the proposed transmitter eliminates the conventional electrical transmitter's massive size and excessive power requirements, allowing efficient and portable wireless communication in the RF-denied environment such as the earth's surface to under-water or deep-water facilities. It is also observed that the operating bandwidth, distance, and efficiency of the AMEBA transmitter can be increased significantly by using an HP-UHSM. It is the main motivation for designing this 2 kW 500 krpm UHSM. The machine specifications are derived from the antenna's communication and system requirements. The antenna is aimed to transmit at least 50 characters per minute in a distance of about 1 km with a bandwidth up to 8333 Hz. Based on the calculations, an UHSM is needed with a shaft torque of 38.2 mNm at 500 krpm. Also, it should not have any bending resonance frequency below 8333 Hz and have a good DSM with high efficiency.

To design this HP-UHSM, a multi-objective optimization is performed using the proposed optimization process, where several multi-disciplinary design constraints are applied based on the application requirements, material limitations, and practical considerations. It has three optimization objectives which are defined as:

$$\begin{cases} f_1(x) = Seck\ target\ of\ 38.2\ mNm\ at\ 500\ krpm \\ f_2(x) = Minimize\ P_E = P_{cu} + P_{Fe} + P_{rotor} \\ f_3(x) = Minimize\ P_f \end{cases}$$

The first objective is defined to achieve the 38.2 mNm shaft torque at 500 krpm. The other two objectives are minimizing the total electrical loss and windage loss separately. The electrical loss consists of copper ohmic loss, copper proximity loss, stator core loss, and rotor eddy current loss. Besides, nine multi-disciplinary constraints are applied to

ensure a feasible design geometry. The multi-disciplinary design constraints are declared as:

$$\begin{cases} g_1(x) = B_{P\_stator} < 1.1\,T \\ g_2(x) = J_{den} < 5\ A/mm^2 \\ g_3(x) = P_{den} > 60\ kW/L \\ g_4(x) = T_{W\_max} < 130^0\ C \\ g_5(x) = T_{PM\_max} < 150^0\ C \\ g_6(x) = \sigma_{PM} < 100\ MPa \\ g_7(x) = \sigma_{SL} < \lambda\sigma_{t,SL}\ MPa \\ g_8(x) = p_c > 0\ MPa \\ g_9(x) = \omega_{1st} > 8500\ Hz \end{cases}$$

In electromagnetic analysis, the peak stator flux density (B_p), the current density (J_{den}), and the power density (P_{den}) are constrained based on the material's saturation limit, natural air cooling, and require power density, respectively. In thermal analysis, the maximum temperature of PM (T_{PM}) as well as winding (T_W) are controlled based on the BH_{max} of PM and thermal limit of coil insulation, respectively. In structural analysis, the maximum stress on PM origin (σ_{PM}) and inner sleeve (σ_{SL}) is controlled below their corresponding physical strength limit considering a minimum safety factor (λ). In addition, the interference-fit contact pressure (P_c) is forced to be positive to ensure proper torque transfer. Considering the Rotordynamic, the first undamped bending frequency (ω_{1st}) is restricted above the rated frequency.

The optimization is executed using the multi-objective genetic algorithm (MOGA). It has eight design variables; the upper and lower bounds of these variables are given in Table-I. The optimization is converged after 1154 iterations with a six-phase winding configuration. The optimal candidate point is selected using a trade-off between the total electrical loss and the windage loss. The best candidate is the one that satisfies all the design constraints and has the maximum DSM considering multi-physics performance. The input design parameters of the optimal design point are also given in Table-I. The optimal machine has Sm_2Co_{17} as PM, titanium alloy as the sleeve, amorphous iron as stator core, and Litz wire as winding. The output performances of the optimal design point are given in Table-II. The optimal design has an output shaft torque of 38.35 mNm at 500 krpm with an efficiency of ~94.5%, and it does not have any natural bending frequency below the rated frequency. Moreover, it satisfies all the design constraints with a global DSM of ~30%.

The total computational time is about 4.2 hours for a laboratory desktop of 64-bit, Intel i9, 3.6 GHz CPU with 32 GB RAM. To evaluate the computational efficiency, the optimal DP is simulated using the full FEA model, where a 2-D ANSYS-electronic-desktop, 3-D Fluent-CFD, 3-D steady-state-thermal, 2-D static-structural, and 3-D Modal module are used for electromagnetic, windage loss, thermal, structural, and Rotordynamic analysis, respectively. All these modules are coupled to each other in Workbench. A fine mesh is used in the high stress or critical region, whereas a coarse mesh is used elsewhere. The single simulation takes about 32 minutes using the same computer, whereas the proposed model takes only ~1 minute to solve the DP. Hence, the proposed optimization model is about 30 times faster than the conventional FEA optimization.

Therefore, it is concluded that the proposed optimization model has the capability to optimize and design HP-UHSM by successfully addressing its critical design challenges with significantly reduced computational cost.

Table-I: Input variables and the optimal candidate point

Input and obtained Parameters	Lower bound	Upper bound	Optimal Value
PM radius (R_1) [mm]	2.5	5	3.9
Sleeve thickness (t_{SL}) [mm]	0.25	2	0.7
Stator thickness (t_{ST}) [mm]	1.5	3.5	2.75
Shrink fit length ($\Delta\delta_o$) [µm]	5	40	20
Stack length (L) [mm]	30	60	40
Phase current (I_{rms}) [A]	2.5	10	3.9
Number of turns *(Nc)*	10	40	20
Number of phases *(m)*	3	9	6
Stator inner radius (R_4) [mm]	obtained		11.25

Table-II: Output performances of the optimal candidate point

Output parameters	Value	Unit
Shaft torque at 500 krpm (T_e)	38.35	mNm
Total electrical loss (P_E)	51.2	W
Windage or Air-friction loss (P_f)	61.1	W
Flux density in the stator (B_{st})	0.61	T
Winding current density (J_{den})	4.92	A/mm^2
Power density (including end winding (P_{den})	64.9	kW/L
Maximum PM temperature (T_{PM})	124.6	°C
Maximum winding temperature (T_W)	110.2	°C
Maximum stress on PM ($\sigma_{r,PM}$)	83.3	MPa
Maximum stress on inner sleeve ($\sigma_{t,SL}$)	621.2	MPa
Contact pressure between PM and sleeve (P_c)	80.62	MPa
1st undamped bending frequency (ω_{1st})	9103	Hz

V. FEA Simulation Results

In this section, the optimal design point is analyzed using FEA simulation, and the results are compared with the optimization output performance of Table - II.

A. Electromagnetic analysis

The full machine is simulated using a motoring operation. A six-phase asymmetric toroidal winding with a displacement angle of 30° is implemented in the stator. Each phase coil has 40 turns in series. Fig. 6 shows that when 5.53 A peak sinusoidal current is applied it develops an average electromagnetic torque of 38.24 Nm at 500 krpm, equivalent to 2 kW rated power. Fig. 7 shows the maximum flux density in the stator is 0.61 Wb at the rated current. Also, it has 2.2 W core loss, 48 W copper loss, 0.2 W rotor power loss, and ~60 W windage loss at the rated operation. It is resulting an efficiency of 94.5% considering the electrical and windage loss.

B. Thermal analysis

A 3-D FEA model is used to analyze the temperature distribution of the designed HP-UHSM. The losses are imported from the electromagnetic and windage loss model. Fig. 8 shows the temperature distribution of the machine at rated conditions. The maximum temperature of PM is ~128° C, which is mainly generated by the windage loss. The maximum winding temperature is ~105° C, and the stator core temperature is ~95° C. It is also observed that the temperature distribution on the PM is not linear; rather it increases gradually from the edge to the center of the magnet and follows an axial axis symmetry.

C. Structural analysis

Fig. 9 depicts the VMES distribution on the rotor at a standstill and 500 krpm. The temperature effect is also

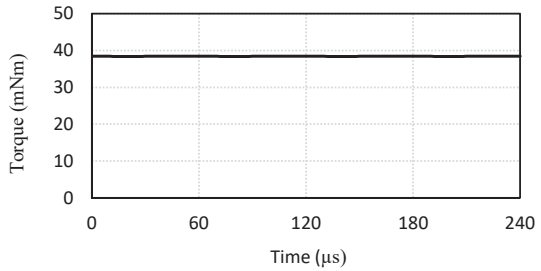

Fig. 6: Electromagnetic shaft torque at 500 krpm.

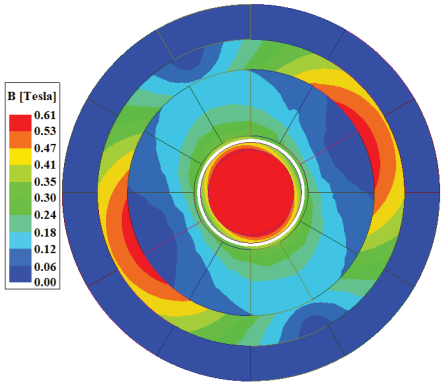

Fig. 7: Flux density distribution at the rated condition.

Fig. 8: Temperature distribution at rated condition.

included to consider the thermal expansion. At a standstill, the PM experiences compressive stress of 82 MPa, and the sleeve experiences a VMES of 538 MPa at the inner edge due to the interference fit implementation. At 500 krpm, the maximum VMES on PM center and sleeve inner edge are 83 MPa and 620 MPa, which are well below the strength limit of the sleeve material. The contact pressure at the interference-fit zone is 82 MPa at a standstill and it becomes 68 MPa at 500 krpm. Therefore, the contact pressure is positive throughout the entire speed region.

D. Rotordynamic analysis

The undamped natural frequency of the proposed rotor is analyzed by the ANSYS modal simulation. A 3-D model is simulated using a free-free boundary condition. The rotor has a first-order bending mode at 9012 Hz and a second-order bending mode at 17053 Hz. Fig. 10 shows the rotor deformation at these frequencies. These frequencies will further move to high frequency when the guide bearing is installed. A detailed Rotordynamic of this rotor is presented in [21].

The FEA results show very good agreement with the Multiphysics output performance (Table-II) of the optimization model. The comparative error between the analytical and FEA model is only 1 to 3%, which is acceptable. Therefore, the analytical models are accurate enough to optimize and design an HP-UHSM.

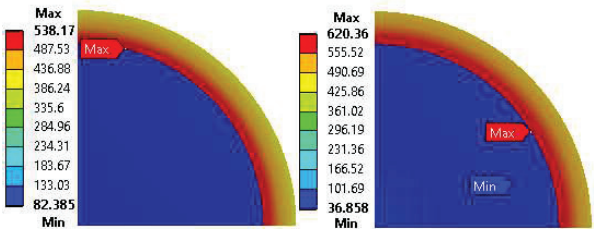

Fig. 9: Structural analysis (left) at standstill, (Right) at 500 krpm.

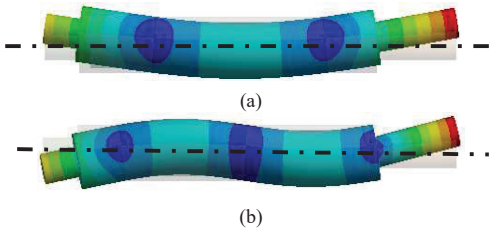

Fig. 10: (a) 1st order (9012 Hz) and (b) 2nd order (17053 Hz) bending mode.

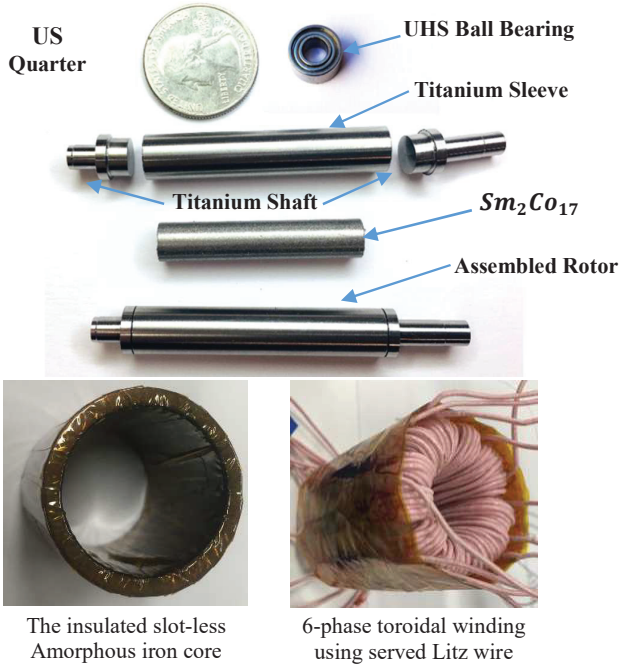

Fig. 11: Rotor and stator parts of 2 kW 500 krpm UHSM prototype.

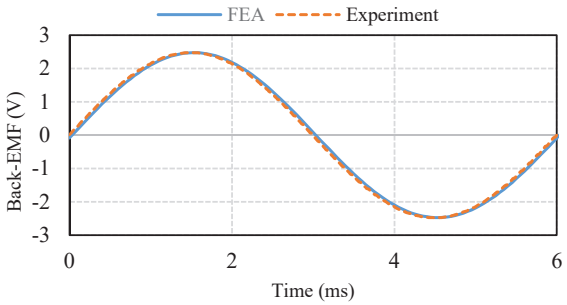

Fig. 12: No load back-EMF of phase-A at 10 000 rpm.

VI. Experimental Results

A prototype of the 2 kW 500 krpm UHSM is built using the optimal geometry parameters given in Table-I. Fig. 11 shows different parts of the prototype. Rotor parts are designed using CNC machining technology with a precision tolerance of ± 0.005 mm. The rotor is assembled using the shrink-fit technique. A pair of customized UHS ceramic ball bearing is used, which can operate at 500 krpm continuously for at least 15 hours. A 6-phase asymmetric toroidal winding is applied on the amorphous stator core. The displacement angle between two 3-phases is 30° electrical. Fig. 12 shows the back-EMF of the prototype at 10 000 rpm. It also shows a comparison between the FEA and experimental back-EMF of phase-A. The experimental result has a back-EMF constant of 2.5×10^{-4} V/rpm, which is closely agreed with the FEA result. The undamped natural frequency of the rotor is also measured using impulse hammer testing. The experimental value of first and second order bending frequency are ~9248 Hz and ~17125 Hz respectively. The test results match with the FEA result of Fig. 10 with an error of 1.6% only.

VII. Conclusion

In this paper, a new Multiphysics optimization strategy is presented to design HP-UHSM. The optimization method integrates an FEA electromagnetic model with the analytical model of windage loss, structural analysis, thermal analysis, and Rotordynamic analysis. This allows to apply several multi-disciplinary design constraints and to consider the mutual influence of Multiphysics performance variation in HP-UHSM. Therefore, the proposed optimization technique can provide an efficient optimal design with high DSM and significantly reduces the FEA computational cost. The Multi-disciplinary analytical modeling, critical design constraints of HP-UHSM, mutual coupling, and the optimization process are described and discussed in detail. Using the proposed strategy, a 2 kW 500 krpm UHSM is optimized for AMEBA application considering some unique multi-disciplinary design constraints. The effectiveness of the proposed model and its accuracy are verified using the FEA results. The machine has an efficiency of 94.5% with a 30% global safety margin and satisfies all the design specifications. Finally, the design machine is prototyped and tested in the laboratory. The test results show good agreement with the proposed optimization model and FEA results. In the future, full-load operation, full-speed operation, and the AMEBA application of the designed machine will be investigated experimentally.

Acknowledgment

This research was supported in part by the National Science Foundation CCSS-Comms Circuits &Sens System Program (Award # 1905434). Authors appreciate the support from the Center of Advanced Vehicular Systems at Mississippi State University.

References

[1] N. Uzhegov, E. Kurvinen, J. Nerg, J. Pyrhönen, J. T. Sopanen and S. Shirinskii, "Multidisciplinary Design Process of a 6-Slot 2-Pole High-Speed Permanent-Magnet Synchronous Machine," in IEEE Transactions on Industrial Electronics, vol. 63, no. 2, pp. 784-795, Feb. 2016.

[2] C. Zwyssig, J. W. Kolar and S. D. Round, "Megaspeed Drive Systems: Pushing Beyond 1 Million r/min," in IEEE/ASME Transactions on Mechatronics, vol. 14, no. 5, pp. 564-574, Oct. 2009.

[3] J. Sim et al., "Multiphysics Design of Triple 3-Phase PMSM for Ultra-High Speed Elevator Applications," 2018 XIII International Conference on Electrical Machines (ICEM), Alexandroupoli, 2018, pp. 284-290.

[4] S. Ruoho, T. Santa-Nokki, J. Kolehmainen and A. Arkkio, "Modeling Magnet Length In 2-D Finite-Element Analysis of Electric Machines," in *IEEE Transactions on Magnetics*, vol. 45, no. 8, pp. 3114-3120, Aug. 2009

[5] P. Asef, R. B. Perpiñà, M. R. Barzegaran, A. Lapthorn and D. Mewes, "Multiobjective Design Optimization Using Dual-Level Response Surface Methodology and Booth's Algorithm for Permanent Magnet Synchronous Generators," in *IEEE Transactions on Energy Conversion*, vol. 33, no. 2, pp. 652-659, June 2018,

[6] C. Zwyssig, J. W. Kolar, W. Thaler and M. Vohrer, "Design of a 100 W, 500000 rpm permanent-magnet generator for mesoscale gas turbines," Fourtieth IAS Annual Meeting. Conference Record of the 2005 Industry Applications Conference, 2005., Kowloon, Hong Kong, 2005, pp. 253-260.

[7] T. Baumgartner, R. M. Burkart and J. W. Kolar, "Analysis and Design of a 300-W 500 000-r/min Slotless Self-Bearing Permanent-Magnet Motor," in IEEE Transactions on Industrial Electronics, vol. 61, no. 8, pp. 4326-4336, Aug. 2014

[8] F. R. Ismagilov, N. Uzhegov, V. E. Vavilov, V. I. Bekuzin and V. V. Ayguzina, "Multidisciplinary Design of Ultra-High-Speed Electrical Machines," in *IEEE Transactions on Energy Conversion*, vol. 33, no. 3, pp. 1203-1212, Sept. 2018,

[9] *Electromagnetic modeling of power electronic converters*. Norwell, Massachusetts:Kluwer Academic Publishers, 1989, ch. 6.

[10] G. Bertotti (1988), "General properties of power losses in soft ferromagnetic materials", IEEE transactions on magnetics, Vol. 24, No. 1, pp. 621-630.

[11] C. Zwyssig, S. Round, and J. Kolar, "Analytical and experimental investigation of a low torque, ultra-high speed drive system," in *Conference Record of the 2006 IEEE Industry Applications Conference Forty-First IAS Annual Meeting*, 2006, pp.1507-1513.

[12] M. Awad and W. Martin, "Windage loss reduction study for tftr pulse generator," *Fusion Engineering, 1997. 17th IEEE/NPSS Symposium*, vol. 2, pp. 1125 –1128 vol.2, oct. 1997.

[13] M. K. Islam and S. Choi, "Analysis of Axial Temperature Variation Effect on the Performance of Five-Phase Permanent Magnet assisted Synchronous Reluctance Motor," *2020 IEEE Energy Conversion Congress and Exposition (ECCE)*, 2020, pp. 1107-1114

[14] K. Tanimoto, K. Kajihara, and K. Yanai, "Hybrid ceramic ball bearings for turbochargers." *SAE Transactions: Journal of Materials & Manufacturing*, vol. 109, pp. 763–775, 2000.

[15] Gunnar Kylander. Thermal modelling of small cage induction motors. Ph.D. dissertation, Dept. of Electric Power Eng., Chalmers University of Technology, G oteborg, Sweden, 1995.

[16] Z. Huang, J. Fang, X. Liu and B. Han, "Loss Calculation and Thermal Analysis of Rotors Supported by Active Magnetic Bearings for High-Speed Permanent-Magnet Electrical Machines," in *IEEE Transactions on Industrial Electronics*, vol. 63, no. 4, pp. 2027-2035, April 2016

[17] S. Timoshenko and J. Goodier, *Theroy of elasticity*. New York, USA: McGraw-Hill, 1970.

[18] DARPA. *A Mechanical Based Antenna (AMEBA)*. Accessed: Dec. 19, 2016. [Online]. Available: https://govtribe.com/ opportunity/federal-contract-opportunity/a-mechanical-based-antennaameba-hr001117s0007.

[19] J. S. Glickstein, J. Liang, S. Choi, A. Madanayake and S. Mandal, "Power-Efficient ELF Wireless Communications Using Electro-Mechanical Transmitters," in *IEEE Access*,vol.8, pp. 2455-2471, 2020.

[20] M. K. Islam and S. Choi, " Modeling and Design of a 6-Phase Ultra-High-Speed Machine for ELF/VLF Wireless Communication Transmitter," *2021 IEEE Applied Power Electronics Conference and Exposition (APEC), 2021,* in press.

[21] M. K. Islam and S. Choi, "Rotordynamic Analysis of 500 000 r/min 2 kW Ultra-High-Speed Machine for Portable Mechanical Antenna," *2021 IEEE International Electric Machines & Drives Conference (IEMDC)*, 2021, pp. 1-7